AI Medicine
https://www.sciltp.com/journals/aim

Review

Check for updates

Deep Learning-Based Quantification of Epicardial Adipose Tissue: A Review

Jie Teng [1], Yiweng Zhang [1], Jiayi Wang [1] and Qi Zhao [2,*]

[1] School of Medical Imaging, Wannan Medical University, Wuhu 241001, China
[2] Faculty of Information, Liaoning University, Shenyang 110036, China
* Correspondence: qizhao7178@163.com

How To Cite: Teng, J.; Zhang, Y.; Wang, J.; et al. Deep Learning-Based Quantification of Epicardial Adipose Tissue: A Review. *AI Medicine* **2026**, *3*(2), 8. https://doi.org/10.53941/aim.2026.100008

Received: 4 May 2026
Revised:7-30 July 2026
Accepted: 4 August 2026
Published: 15 September 2026

Abstract: Epicardial adipose tissue (EAT) is a potential imaging biomarker of cardiovascular risk. Manual EAT quantification is time-consuming and subject to observer variability. Deep learning (DL) offers tools for faster and more consistent measurements. This narrative review examines DL approaches to EAT quantification, their anatomical foundations, imaging applications, and clinical validation. We start with the definition of EAT to establish the clear anatomical and embryological differences between EAT and other fat depots (paracardial fat) to ensure accurate AI model construction. We then outline the advancements made in DL architecture development, from traditional U-Net models to advanced ones combining CNN and Transformers with regard to global features acquisition, including new models such as Mamba, which enables higher computation efficiency. Finally, we analyze how these models perform in different imaging techniques, focusing specifically on CT and MRI imaging. Reported segmentation performance varies with the imaging modality, anatomical target, dataset, and evaluation protocol. Although several models show good agreement with expert annotations, external validation and integration across hospital systems remain important challenges. Beyond volume, EAT attenuation and tissue characteristics may provide complementary information for cardiovascular risk assessment. Their clinical use requires reproducible measurements and validation in the intended patient population.

Keywords: epicardial adipose tissue (EAT); deep learning; cardiovascular risk; image segmentation; artificial intelligence; clinical workflow

1. Introduction

Cardiovascular diseases (CVDs) are the top cause of death internationally [1]. Recent research demonstrates that the risk of CVD is linked not only to total body fat, but also to the site and physiological functions of fat [2]. One of the tissues depositing fat in the heart is EAT, which has become the object of research due to its specific location. EAT is situated between the heart muscle and the visceral pericardium, directly contacting both myocardium and coronary arteries. In the absence of a separating fascia [3], EAT directly modulates cardiac function through paracrine and vasocrine pathways, thereby playing a critical role in both physiological and pathological processes [4].

EAT has metabolic, mechanical, and thermogenic functions [5]. Human EAT expresses uncoupling protein 1 (UCP1) and exhibits beige adipose tissue features, suggesting a potential role in local thermogenesis [6,7]. These properties should be distinguished from its roles in lipid handling and mechanical cushioning.

Metabolic disorders can alter the phenotype and secretory profile of EAT [8]. In obesity and related conditions, pro-inflammatory signaling and adipose tissue remodeling may impair its physiological functions [9,10]. EAT abnormalities have been associated with coronary atherosclerosis, atrial fibrillation, and heart failure [11–13].

Because of its important role in health problems, the precise measurement of EAT volume and density has emerged as an essential tool for estimating cardiovascular risk. Knowing the EAT amount helps to identify the

pathogenetic mechanisms involved and provides reliable biomarkers for risk classification in clinical practice [14]. Even though CT and MRI are among the most widely used imaging methods, EAT quantification has relied on manual segmentation as a method that is time-consuming and subject to intra- and interobserver variability [15]. Deep learning-based automated analysis can provide precise and accurate EAT quantification techniques. Compared with manual analysis, deep learning-based methods can improve consistency and reduce variability among analysts [16]. For example, the work by Commandeur et al. shows that the fully automated framework gives high agreement with experts' quantifications (median Dice score of 0.823), thus demonstrating its accuracy [17].

Automated EAT measurements may support research on cardiovascular and metabolic risk, although clinical decision-making requires validation beyond segmentation performance [18, 19]. Studies suggest the possibility of using EAT amount and density for improving the accuracy of coronary artery calcium scores and determining cardiovascular risk [20]. Findings gathered during the COVID-19 pandemic suggest that EAT might play an important role in damage to the heart caused by the virus [21]. This shows that EAT is an important target for both cardiovascular and metabolic diseases.

Recent studies have reported promising performance for automated EAT segmentation, including deep attention networks for CCTA and dedicated methods for non-contrast CT [22, 23]. Their accuracy and computational requirements should be assessed separately for each dataset and deployment setting; results from a single study do not establish a universal performance threshold.

The scope and organization of this review are summarized in Figure 1.

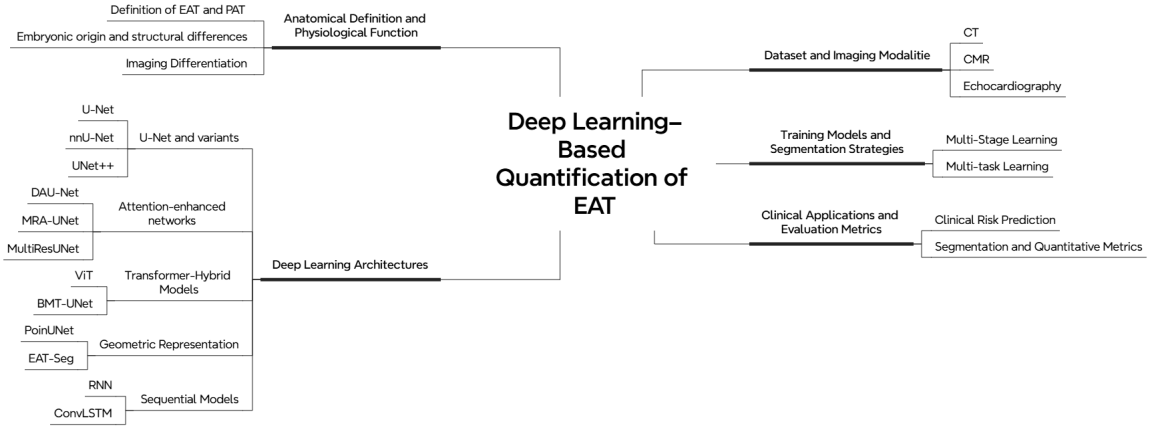

Figure 1. Overview of the research framework for deep learning-based EAT quantification. Abbreviations: BMT-UNet, boundary-enhanced multi-scale U-Net with a convolutional Transformer; ConvLSTM, convolutional long short-term memory; DAU-Net, 3D deep attention U-Net; EAT, epicardial adipose tissue; EAT-Seg, epicardial adipose tissue segmentation network; MRA-UNet, multiscale residual channel attention U-Net; MultiResUNet, multi-residual U-Net; nnU-Net, no-new-U-Net; PoinUNet, Poincaré-guided geometric U-Net; RNN, recurrent neural network; UNet++, nested U-Net architecture; U-Net, U-shaped convolutional network; ViT, vision Transformer.

2. Cardiac Adipose Tissue: Anatomical Definitions and Distinctions

2.1. Anatomical Definitions of Cardiac Fat Depots

Terminology for adipose tissue surrounding the heart has varied across anatomical and imaging studies [24,25]. In particular, pericardial fat has been used for different combinations of epicardial and extra-pericardial depots [26,27]. A study's anatomical definition and segmentation boundary should therefore be stated explicitly.

Imaging also contributes to this ambiguity because the thin pericardium can be difficult to delineate, particularly when little surrounding fat is present [28, 29]. Carr and Ding discussed the use of pericardial fat for a combined depot and reported a strong correlation with EAT volume [24]. Correlation between these measures does not make their anatomical definitions interchangeable.

In this review, EAT denotes adipose tissue between the myocardium and the visceral pericardium; paracardial fat denotes extra-pericardial adipose tissue outside the parietal pericardium [30,31]. To avoid ambiguity, PAT is used for pericardial adipose tissue only when reporting studies that explicitly use this term, and the measurement is specified. EAT and paracardial fat differ in anatomical relationships and biological characteristics [31]. Figure 2 illustrates these compartments.

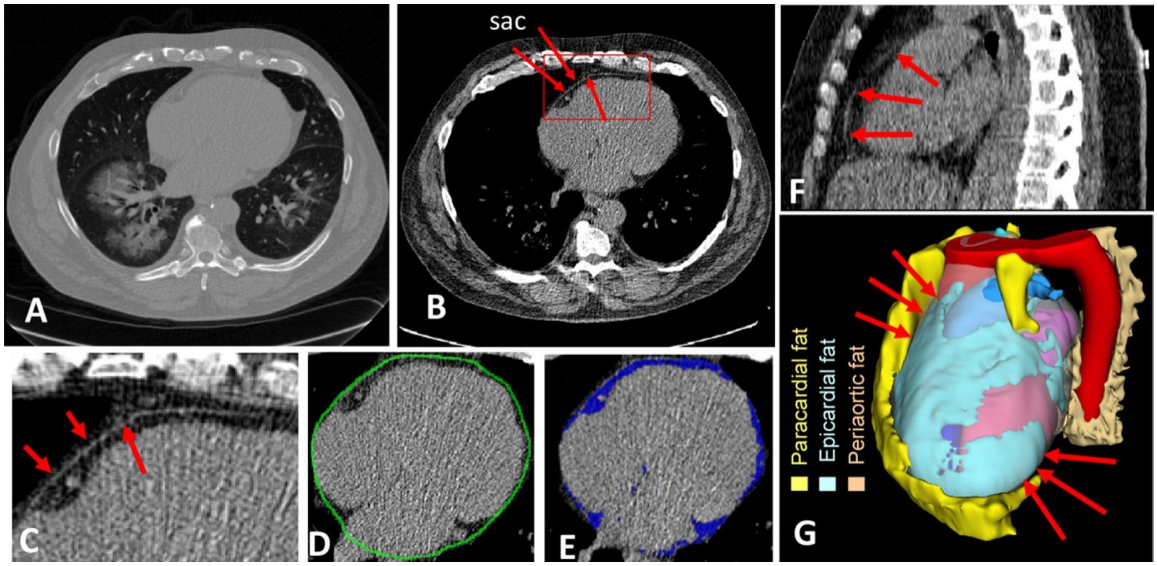

Figure 2. Manual segmentation protocol and 3D anatomical distribution of cardiac adipose depots. (**A**) Representative 2D axial non-contrast CT slice. (**B**) Enhanced visualization of the pericardium using a Hounsfield Unit (HU)-attention window (window width/level: 350/40 HU); arrows indicate the pericardium in the inferior region. (**C**) Magnified view of the red ROI in panel (**B**). (**D**) Expert manual tracing of the pericardium boundary (green contour). (**E**) Final segmentation of epicardial adipose tissue (EAT, blue mask) derived by thresholding interior voxels within the standard fat attenuation range ([−190, −30] HU). (**F**) Supplementary sagittal view for disambiguating pericardial borders in challenging regions. (**G**) 3D spatial rendering illustrating morphological distinctions among cardiac fat depots: EAT (cyan) strictly bounded by the pericardial sac (transparent white), paracardial fat (yellow) located extra-pericardially, and periaortic fat (light brown) surrounding the thoracic aorta (red) [23].

2.2. Embryological Origins and Structural Differences

EAT and extrapericardial fat have entirely different embryonic origins. EAT develops from the splanchnopleuric mesoderm making it an extension of visceral fat since both tissues originate from the same embryonic origin. This is the reason for the ability of EAT to have brown/beige adipose tissue-like qualities giving it high metabolic activity and thermogenic ability [32]. On the other hand, the extra-pericardial fat arises from the primitive thoracic mesenchyme and falls under the category of white adipose tissue making it more similar to subcutaneous fat regarding its metabolic characteristics [33].

EAT directly contacts the myocardium and epicardial coronary arteries without an intervening fascial barrier, enabling local biochemical signaling [34]. Pericoronary adipose tissue (PCAT) is the regional portion of EAT immediately surrounding the coronary arteries, rather than a separate outer layer. More generally, perivascular adipose tissue refers to fat adjacent to blood vessels and is not restricted to the heart. Outside the parietal pericardium lies paracardial fat. These spatial relationships should guide imaging labels and quantitative measurements [30].

The differences in blood supply further strengthen the functional distinction between epicardial adipose tissue (EAT) and extra-pericardial fat. The blood supply of EAT is directly provided by the branches of the coronary arteries, and it shares the same microcirculatory network as the myocardium [5]. This structural feature establishes the foundation for EAT to directly influence the myocardium and coronary arteries through paracrine and vasocrine mechanisms. Extra-pericardial fat gets its blood supply from non-coronary sources, mainly the pericardiophrenic artery, a branch of the internal mammary artery. This means that the impact of extra-pericardial fat on the heart is expected to occur through the general mechanisms rather than by means of direct local actions [32,35].

2.3. Imaging Differentiation and Functional Pathophysiology

Imaging differentiation of these depots depends on identifying the pericardium. Echocardiography measures EAT thickness over the right ventricular free wall, but limited visualization of the pericardial boundary may lead to confusion with paracardial fat [24,29]. CT provides high spatial resolution, while CMR offers complementary soft-tissue contrast. Both can quantify EAT when the relevant boundaries are delineated; the preferred method depends on the acquisition protocol and clinical objective.

EAT provides mechanical cushioning around the coronary arteries [36]. It also participates in local lipid metabolism: hydrolysis of stored triglycerides releases free fatty acids that can be used by the myocardium. EAT secretes adipokines, including adiponectin, whose effects depend on the tissue's metabolic and inflammatory state [37].

These physiological functions should be distinguished from altered signaling in cardiometabolic disease.

In metabolic disorders like diabetes and obesity, EAT's role as a protector turns into a pathological one. EAT starts secreting high amounts of pro-inflammatory cytokines and adipokines that invade the walls of coronary blood vessels, causing atherosclerosis, fibrosis, and arrhythmias development [38]. Numerous studies have indicated that EAT's thickness or volume has an independent correlation with coronary artery calcification, serious adverse cardiovascular incidents, and heart failure [39].

The interpretation of extra-pericardial fat should account for its relationship to overall adiposity and the covariates included in a study's analysis [40,41]. Its clinical associations should not be assumed to be identical to those of EAT.

These distinctions matter for biomarker development: EAT has a local anatomical relationship with the myocardium and coronary vessels, whereas extra-pericardial fat represents a different depot. The incremental value of either measurement must be evaluated for the specific population and clinical outcome.

In imaging quantification, it is critical that annotations and model results take into account anatomical boundaries. Combining intra- and extra-pericardial fat into a generic "pericardial fat" class runs the risk of reducing crucial pathophysiological information from epicardial fat and resulting in algorithms focusing on general obesity instead of specific cardiac risk. Through the use of accurate pericardial outlines in annotation and limiting AI models to epicardial depots, automatic EAT measurement keeps a clear biological significance that improves the understanding of AI-derived metrics as well as their applicability in cardiovascular risk assessment and prediction of outcomes.

3. Imaging Techniques and Clinical Applications

3.1. Imaging Modalities and Quantitative Metrics

Epicardial adipose tissue (EAT) has gained significance as a useful imaging biomarker in heart diseases, as accurate quantification is useful in risk stratification, diagnosis and prognosis. Various imaging methods can be used to measure EAT, but computed tomography (CT) is the most dominant due to its excellent spatial resolution and reliable anatomical outline.

CT can quantify three-dimensional EAT volume and attenuation using protocol-specific segmentation boundaries and fat thresholds, commonly −190 to −30 HU. EAT attenuation is influenced by tissue properties and image acquisition, and should not be treated as a direct measurement of inflammation. In patients with COVID-19, higher attenuation was associated with adverse outcomes [42]. Volume and attenuation should be interpreted together with the imaging protocol and clinical context.

Multidetector CT supports EAT assessment with both non-contrast and contrast-enhanced protocols [43,44]. ECG gating can reduce motion, but neither gating nor contrast administration is required for every validated EAT analysis workflow. Ionizing radiation remains a consideration when acquiring CT specifically for this purpose; opportunistic analysis of existing scans does not require an additional acquisition.

Deep learning developments are now expanding the range of CT datasets suitable for EAT quantification. In an AI-based assessment using data from the SCOT-HEART trial, EAT volume derived from coronary computed tomography angiography (CCTA) was positively associated with future myocardial infarction in cardiometabolic patients [45]. Moreover, deep learning approaches have proven feasible for extracting EAT metrics from low-dose computed tomography (LDCT). In heavy smokers undergoing lung cancer screening, AI-derived EAT parameters linked directly to cardiovascular risk, suggesting that LDCT could also be useful for opportunistic cardiovascular risk evaluation [46]. Figure 3 shows a brief summary of a fully automated deep learning framework that applies predefined attenuation thresholds (−190 to −30 HU) to non-contrast LDCT. Developments like these enable EAT evaluation across large clinical CT datasets without additional image acquisition or radiation exposure.

CMR can quantify EAT without ionizing radiation, and dedicated non-contrast sequences support repeated assessment [47]. Dixon water-fat separation provides complementary image contrasts for EAT segmentation and reconstruction [48]. More specialized acquisition and signal-modeling methods can estimate fatty acid composition [49]; these measurements should not be equated with routine Dixon imaging or direct inflammatory biomarker assays.

Traditionally, studies of epicardial adipose tissue (EAT) have concentrated on its volume and composition; however, recent work has begun to examine its intrinsic tissue characteristics using quantitative techniques originally developed for the myocardium. For instance, T1 mapping is a standard method for quantifying diffuse myocardial fibrosis and inflammation. Applying this parameter to cardiac fat, researchers have shown in a prospective observational CMR registry that EAT T1 relaxation time is independently associated with a composite endpoint of nonfatal myocardial infarction, heart failure hospitalization, and all-cause mortality [50]. These findings indicate that characterization of EAT tissue properties provides valuable prognostic information beyond conventional volumetric assessments [50].

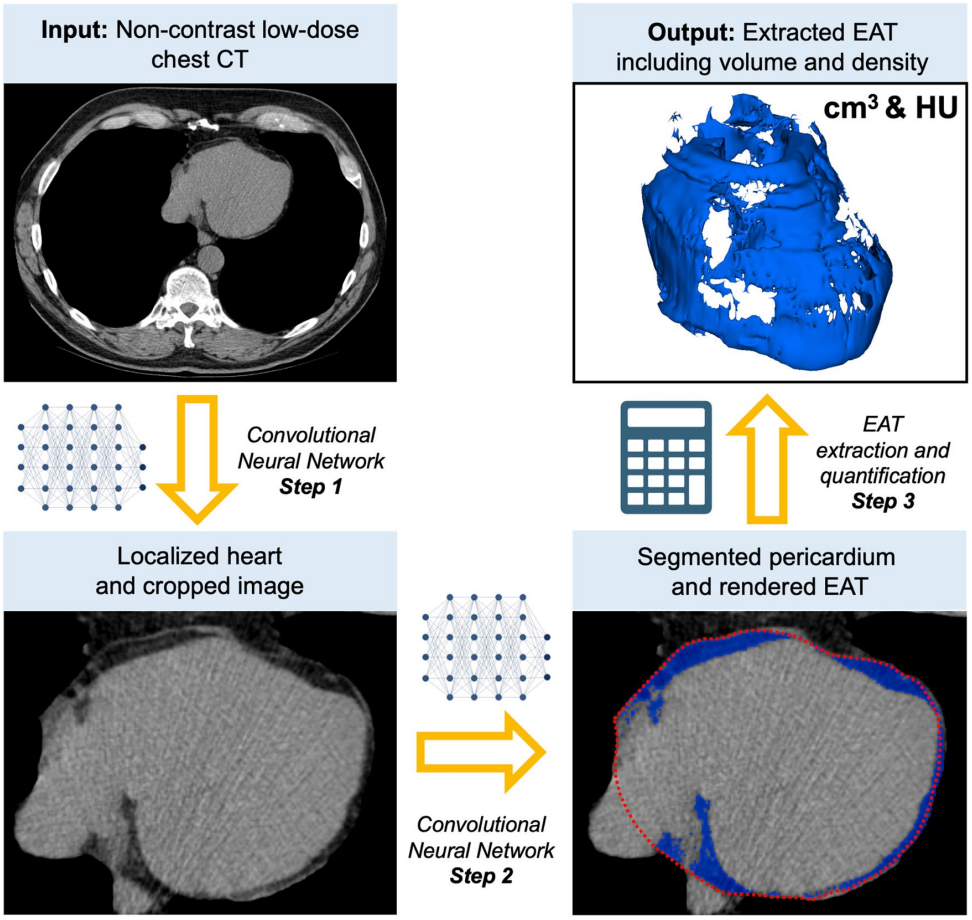

Figure 3. The fully automated deep learning framework for EAT quantification on non-contrast, low-dose lung cancer screening CT scans. The process involves heart localization, pericardial sac segmentation (indicated by the red line), and the extraction of epicardial fat based on predefined attenuation thresholds (−190 to −30 HU) [46].

Multiparametric CMR can evaluate different cardiac structures in the same examination. Skoda et al. used a 3D late gadolinium-enhanced Dixon approach to assess left atrial fibrosis and EAT volume [51]. Zamani et al. reported a correlation between fat area measured on a single horizontal long-axis cine image and three-dimensional CT fat volume [52]. This association does not establish that a single-slice area measurement can replace volumetry without error.

Transthoracic echocardiography (TTE) is an effective and affordable method of medical imaging that is often employed to evaluate epicardial adipose tissue (EAT). As shown in Figure 4, EAT is visualized as an echo-free region that can be found between the outer myocardium and the visceral side of the pericardium. Parasternally measured end-systolic EAT thickness, perpendicular to the right ventricle's free wall, is taken by averaging the values of three cardiac cycles [53]. This technique can be performed easily without the need for radiation.

Echocardiographic measurements do have some limitations based on the dimensional aspect of echocardiography. Measurement of fat thickness alone does not give the complete measurements of body fat mass. Moreover, operator's skills, quality of the acoustic environment and the health condition of the patient affect the use of echocardiography [54]. According to a study done by van Woerden et al. among patients with heart failure, echocardiographic EAT thickness was poorly associated with EAT mass as determined by CMR ($R^2 = 0.38$, $P < 0.001$) [55] indicating that measurement of thickness in a 2D plane is not enough for determining the amount of tissue present. However, TTE can be very beneficial in on-site diagnostic and large-scale epidemiological survey.

The equivalence of EAT metrics in imaging methods is a matter of concern in the clinical and research settings. Although CT and CMR provide comparably good estimates of volumetric EAT, the absolute results may vary due to differences in the imaging techniques and tissue contrast [47]. Meanwhile, echocardiographic wall thickness provides a weak correlation with EAT volumes obtained via CT and CMR due to different measurements and limitations of sonography [54]. Therefore, consistency in the method of imaging should be maintained for longitudinal assessments to limit any systematic error.

Modality selection should be guided by clinical objectives, patient characteristics, and resource availability. CT and CMR are preferred when precise volumetric quantification or tissue characterization is required. Conversely, TTE is appropriate for initial screening, bedside assessment, or population-based studies where accessibility and

feasibility are priorities [56]. As multi-modality imaging continues to advance, complementary strengths across techniques may further enhance the clinical utility of EAT quantification.

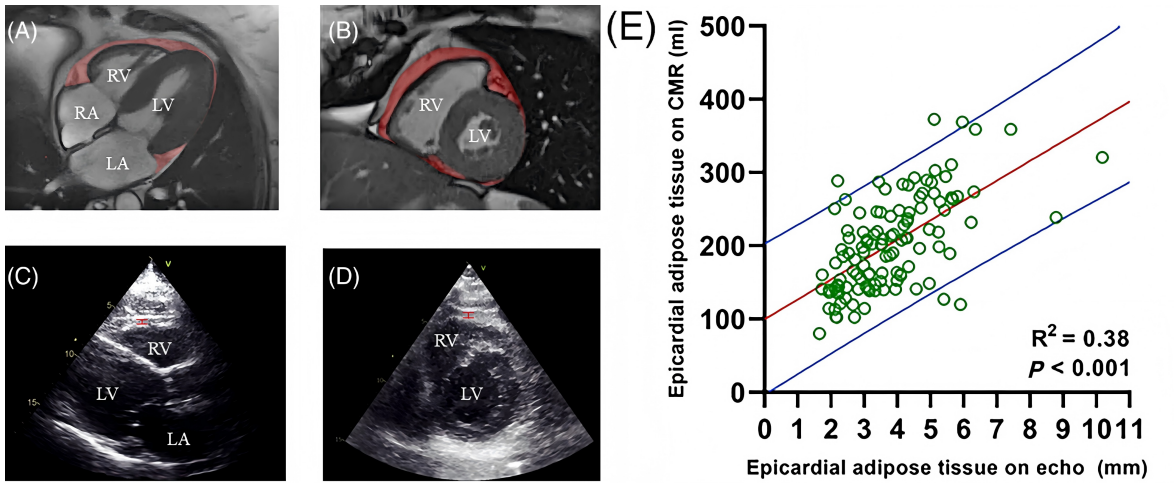

Figure 4. CMR and echocardiographic assessment of EAT. (A, B) CMR examples in four-chamber and short-axis views. (C, D) Echocardiographic thickness measurements in parasternal long-axis and short-axis views. (E) Relationship between CMR-derived EAT mass (g, as labeled on the ordinate) and echocardiographic thickness (mm), with a fitted regression line and prediction intervals. Adapted from van Woerden et al. [55]. Abbreviations: LA, left atrium; LV, left ventricle; RA, right atrium; RV, right ventricle.

Manual annotation remains an important reference for evaluating automated EAT measurements, but requires time and is subject to observer variability. Dedicated CT and CMR segmentation methods can reduce analysis time [17,57]. Their performance must be evaluated for each modality and anatomical target rather than assumed to generalize across all cardiac images.

The principal outputs, strengths, and limitations of CT, CMR, and TTE are compared in Table 1.

Table 1. Comparison of imaging modalities for epicardial adipose tissue quantification.

Modality	Primary Output	Strengths	Limitations	Citations
CT	EAT volume; attenuation	High spatial resolution; reliable pericardial delineation; density-based characterization; scalable automated analysis	Ionizing radiation; protocol-dependent variation; boundary ambiguity in low-contrast or non-gated scans	[27,43]
CMR	EAT volume; tissue composition	Radiation-free; superior soft-tissue contrast; longitudinal follow-up; multiparametric characterization	Longer acquisition time; higher cost; lower availability; limited annotated datasets	[47]
TTE	Linear EAT thickness	Widely available; inexpensive; bedside applicable; suitable for screening and epidemiological studies	Operator-dependent; two-dimensional measurement; limited agreement with true volumetric EAT burden	[53,56]

3.2. Clinical Validation and Prognostic Efficacy

Aside from refining segmentation accuracy through engineering metrics, proper application of deep learning techniques for EAT recognition depends on trials in multiple centers to assess the method's prognostic significance, which is needed for related cardiovascular risk assessment.

Automated EAT measurements have been evaluated in several clinical settings, including lung cancer screening and the SCOT-HEART trial [45,58]. In a multicenter myocardial perfusion imaging cohort, Miller et al. found that higher EAT volume and higher attenuation from low-dose CT were independently associated with the composite

outcome of death or myocardial infarction [59]. This result should be interpreted within the population and acquisition protocol studied.

In CMR, Guglielmo et al. evaluated an EAT volume index normalized to height in patients undergoing stress CMR and reported an association with adverse cardiovascular outcomes [60]. The definition of the index and the clinical endpoint should be retained when comparing prognostic findings across studies.

In addition, the clinical concept of opportunistic automated EAT assessment is now being applied in acute systemic inflammatory processes. Automated low-dose chest CT protocols have successfully linked EAT attributes to the severity pattern of pulmonary involvement and later clinical worsening while treating hospitalized cohorts with acute pneumonia or COVID-19 [61]. These findings support further evaluation of automated EAT measurements as imaging biomarkers; they do not establish autonomous clinical risk assessment.

4. Deep Learning Approaches for EAT Quantification

4.1. U-Net and Its Variants

Before deep learning was introduced, epicardial adipose tissue was mainly quantified through rule-based image processing and classical machine learning (ML) techniques. Various studies using early CT scans implemented fixed Hounsfield unit thresholds for identifying adipose tissues inside pericardial contours that were drawn either manually or semi-automatically. Sometimes, simple region growing and morphological techniques were combined with the procedure. Some researchers relied on supervised ML techniques like random forests and regression models to predict volumes of fat in the pericardial and mediastinal regions. These methods were among the first to carry out systematic measurements of epicardial and pericardial fat in a variety of patient populations; however, these methods depend a lot on manual rules and the expertise of the operator for successful completion. In addition, the methods can fail to offer reliable measurements for different scans based on the protocol or equipment used. The modern deep learning methods, described in the next section, offer a solution to this problem since they focus on training models that are able to outpace both heuristic pipelines and be more reliable, replicable, and scalable.

Early approaches to cardiac fat quantification included conventional machine learning and threshold-based processing [62,63]. CNN-based methods subsequently enabled automated segmentation in CT and CMR, although performance varies with the acquisition and target. Tang et al. reported median DSCs of 0.916 for 2D evaluation and 0.896 for 3D evaluation in CCTA [64]; Feng et al. reported a DSC of 0.881 using Dixon MRI [48]. These study-specific values do not imply that all methods exceed a common accuracy threshold.

The encoder-decoder model and skip connections of U-Net made the base for the further EAT segmentation algorithms development. Geers et al. presented a fully automated 3D U-Net model based on the nnU-Net architecture which was applied to the coronary CT angiography (CCTA) data of 1770 patients involved in the SCOT-HEART experiment [45]. The study proved that deep learning approaches can extract EAT volume and attenuation data from heterogeneous data sources effectively and reliably without needing manual intervention to solve the problem of time-consuming and inconsistent manual delineation. Their findings attest to the reliability of the U-Net architecture in clinical research of a larger scale. Although 3D volumetry characterizes the full depot, 2D measurements may offer practical advantages for selected applications. According to Theis et al. [65], 3D segmentation is challenged by high inter-observer variability because the pericardial boundary does not always have a consistent visibility across full-heart scans. Therefore, they created an end-to-end 2D pipeline that applies reinforcement learning to determine the aortic valve (AV) position. Anatomical markers at this position were shown to be unique, with measurements of the area of EAT done through AI-based techniques having a high reliability with manual gold standards ($r = 0.96$) as well as a better ability to segment (Dice 0.913) than some known 3D techniques like the open-source body and organ analysis (BOA). This implies that 2D measurements can be useful substitutes for costly and strenuous 3D total segmentation in large volume screening processes.

Standard algorithms have limited efficacy in delineating the pericardial layer in the lower and top parts of non-contrast CT due to low contrast and ambiguous anatomical borders. Zhou et al. (2018) introduced the UNet++ architecture [66] to address the semantic gap from the extended skip connections of the traditional U-Net model. UNet++ uses nested structure and dense pathways to better extract and utilize features at different scales. Following that, Leng et al. (2025) advanced a better version of 3D UNet++ [67]. Different from the current slice-wise 2D segmentation, this model utilizes the three-dimensional context of the data. To solve the mentioned issue of blurred boundaries, the study proposed a "redundant class strategy," using additional classes to enhance the model's differentiation concerning blurry boundaries of lower slices. The model was successfully validated during the APOLLO trial which used multi-center and multi-ethnic data with a mean DSC of 0.922 and a mean relative volume error of 4.84% in the internal validation cohort.

4.2. Integration of Attention Mechanisms and Residual Learning

Although the U-Net model shows great results in medical image segmentation, it suffers from low performance when segmenting small structures with complex shapes such as epicardial adipose tissue (EAT). The solution to this problem is the use of attention and multi-scale feature fusion techniques. In their research paper, He et al. [22] proposed the use of the 3D Deep Attention U-Net model (DAU-Net) that utilizes Attention Gates (AGs) in order to segment the complicated anatomy of EAT in coronary CT angiography (CCTA) scans. This model integrates AG modules in skip connections and uses semantic information provided by deep features as gating signals to suppress irrelevant noises and enhance the features of irregular edges of EAT at the same time, improving the accuracy of segmentation of fine structures dramatically.

To bridge the "semantic gaps" due to the simple joining of low-level and high-level features in a conventional U-Net, the modified MRA-UNet was created [68]. The system uses a Multiscale Concatenate Module (MSC) that employs Atrous Spatial Pyramid Pooling (ASPP) for gathering multi-scale contextual information, thus compensating for the loss of spatial information through pooling and connecting features of varying semantic levels. Importantly, the architecture uses a Residual Channel Attention (RCA) approach to modify channel weights (channel re-weighting) to emphasize the most important features and remove those that do not contribute significant information. Bard et al. (2021) applied MultiResUNet to single-slice pericardial adipose tissue area on four-chamber CMR images [69]. This model uses MultiRes Block instead of regular convolutions which manages to increase model performance in terms of multi-scale feature extraction. Importantly, the work proposed using permanently active dropout layers (rate = 0.3) in the encoder and decoder paths, hence making it possible for the network to perform Monte Carlo Sampling during inference. This innovation allows the generation of several predictive samples from a single input signal, so it can be used for estimating epistemic uncertainty of segmentation, leading to an ex ante internal quality assessment of results and helping to identify segmentation outputs with low quality.

4.3. CNN-Transformer Hybrid Architectures

Hybrid CNN–Transformer architectures combine local feature extraction with modeling of longer-range spatial relationships. In order to overcome the issues concerning complexities brought about by EAT distribution in cardiac MRI, Ye et al. (2024) have developed a hybrid architecture based on the Vision Transformer (ViT) [70]. While the base of this model is a ViT for dealing with 2D images using attention blocks, a 2D-pretrained ViT requires adaptation to exploit volumetric context. In order to solve this problem, the research developed an innovative solution called the 3D Adapter modules, creating a 2D and 3D pre-training model. The use of 3D convolutional layers in adapters for the extraction of inter-slice features helps combine local 3D spatial awareness of CNNs with global attention of Transformers. This made it possible to achieve 0.767 DSC. In the arena of coronary CT angiography (CCTA), where efficiency is crucial, Boundary-Enhanced Multi-scale U-Net with a Convolutional Transformer (BMT-UNet) was developed by Wang et al. (2025) using Convolutional Transformer (ConvT) modules in order to eliminate "internal holes" in segmentation masks caused by limited receptive fields of standard CNN architectures [71]. The key advancement of this research is the use of convolutional layers in place of traditional linear projections for the extraction of queries (q), keys (k) and values (v). The proposed idea captures long-range spatial dependencies as well as preserves important local spatial features efficiently. The utilization of a weighted multi-slice method contributes into achieving a favorable capability of the suggested framework to use continuity across slices. Thus, it was revealed that the suggested method achieves a DSC of 0.939 as well as a volume correlation coefficient of 0.99 on CCTA data, which enhances the reliability of large clinical studies results.

Recent research is increasingly utilizing modern mathematical theories in addition to the traditional CNN and Transformer framework to deal with the geometric characteristics of complex anatomy and improve the computational processing of high dimensional data. According to Firouznia et al. (2025), existing methods based on Euclidean space convolutions will not bring satisfactory results due to the complexity of the hierarchical structure of the EAT surrounding the left atrium. Hence, the authors introduced PoinUNet which is a variation of 3D U-Net with Poincaré embeddings layer [72]. The model utilizes the hyperbolic space's negative curvature to transform features through Möbius operations into the Poincaré ball. This non-Euclidean embedding technique greatly enhances the model's ability to process complex spatial structures and anatomical hierarchies and results in significantly higher segmentation effectiveness on Dixon MRI (DSC 0.87) than the Transformer-based approach of SwinUNETR. Optimizing geometric representation does not eliminate the problems of multi-modal data processing. Feng et al. developed EAT-Seg, using Mamba architecture to avoid high computational costs of Transformers [48]. This technology is based on Res-Mamba module and Selective State space models, allowing modeling of long-range spatial dependencies with low complexity. In this research, an input-level fusion method was introduced in multi-phase Dixon imaging that used signed distance maps for shape-based segmentation. The effectiveness of State Space Models in medical image segmentation is

confirmed by the high accuracy of the current work (DSC 0.881). The datasets, imaging modes, sample sizes, and reported Dice scores of the reviewed architectures are summarized in Table 2.

Table 2. Study-specific cohorts and reported measurements for automated cardiac fat analysis.

Method	Imaging	Reported cohort	Target and reported result	Ref.
ConvLSTM + thresholding	NCCT	8781 total; 500 development	EAT volume/attenuation; prognostic cohort (DSC not summarized)	[59]
RL-Medical + 2D U-Net	CECT	1552	EAT quantification (DSC not summarized)	[65]
3D U-Net	CCTA	1770	EAT volume; prognostic cohort (DSC not summarized)	[45]
3D U-Net	CECT	157	Total EAT: 0.870 ± 0.027; LA-EAT: 0.846 ± 0.057; RA-EAT: 0.841 ± 0.071	[73]
3D U-Net	LDCT	24,008	EAT measures; mortality cohort (DSC not summarized)	[74]
DeepHeartSeg	LDCT	20,661	Serial EAT measures; mortality cohort (DSC not summarized)	[58]
DeepHeartSeg	LDCT	24,090	Heart mask median DSC: 0.95; this is not an EAT DSC	[46]
3D UNet++	NCCT	1403 total; 250 internal validation	Internal EAT mean DSC: 0.922	[67]
Improved U-Net	CMR	150	EAT DSC: 0.7772 ± 0.0253; paracardial fat: 0.7718 ± 0.0354	[75]
MIDL	CCTA	108 total; 60 training, 8 validation, 40 test	EAT median DSC: 3D 0.896 (IQR 0.874–0.908); 2D 0.916 (IQR 0.846–0.948)	[64]
DeepFat + Fat-omics	NCCT	40,851	Segmentation DSC: 0.8852 ± 0.033	[76]
DL volumetry	CMR	730	EAT index; prognostic cohort (DSC not summarized)	[60]
U-Net / FCNB	CMR	100	EAT DSC: U-Net 0.77 ± 0.07; FCNB 0.76 ± 0.07	[57]
3D U-Net (AG + DSV)	NCCT/CECT	260 (220 NCCT; 40 CECT)	Best mean EAT DSC: 0.8902	[77]
DAU-Net	CCTA	200	Median EAT DSC: 0.927	[22]
MultiResUNet	CMR	345 training; 87 test; 45,519 application; 103 external	Single-slice PAT area: test mean DSC 0.80; external mean predicted DSC 0.78 (quality-control estimate)	[69]
MRA-UNet + T-CNN	NCCT	103	Mean EAT DSC: 0.883	[68]
BMT-UNet	CCTA	50	Pericardium DSC: 0.983; EAT DSC: 0.939	[71]
Text-prompted ViT	CMR	79	EAT DSC: 3D 0.767 ± 0.094; 2D 0.762 ± 0.101	[70]
PoinUNet	Dixon MRI	66	Left atrial EAT: multi-label DSC 0.87	[72]
EAT-Seg	Dixon MRI	90	EAT DSC: 0.881; HD95: 3.213 mm	[48]
Dual U-Nets	NCCT	20	EAT DSC: 0.9119	[78]
FM-Net	CMR	90	Mean EAT DSC: 0.863	[79]
Multi-task U-Net + xHRNet	LDCT	353	EAT mean DSC: 0.85 ± 0.05; median: 0.87	[61]
Multi-task CNN + statistical shape model	NCCT	250	EAT median DSC: 0.823 (IQR 0.779–0.860)	[17]

Cohort sizes refer to the populations reported in the studies and do not necessarily represent annotated training sets; known subdivisions are specified. DSC values are on a 0–1 scale. Mean, median, IQR, and predicted quality-control estimates are distinguished where reported. Heart-mask DSC, PAT-area DSC, left atrial EAT DSC, and whole-EAT DSC describe different targets and are not interchangeable. These heterogeneous studies do not provide a direct ranking of architectures. AG, attention gates; CECT, contrast-enhanced CT; CCTA, coronary CT angiography; DSV, deep supervision; HD95, 95th-percentile Hausdorff distance; IQR, interquartile range; LA/RA, left/right atrium; LDCT, low-dose CT; NCCT, non-contrast CT; PAT, pericardial adipose tissue.

Table 2 reports study-specific results. Differences in imaging protocols, target definitions, cohorts, and evaluation procedures preclude a direct ranking of architectures from these values.

4.4. Multi-Stage and Multi-Task

Due to the significant similarity in the CT attenuation of epicardial adipose tissue (EAT) and paracardial adipose tissue, whole-image segmentation techniques tend to misidentify them. To reduce errors caused by extrapericardial tissues and keep segmentation restricted to the cardiac region, many researchers have begun to use cascading methodologies—this is also known as the coarse-fine method. Cascaded networks have also been studied in pancreas segmentation [80]. For EAT quantification, Zhang et al. (2020) proposed a Dual U-Nets framework [78]. This model uses a two-stage cascading system. The first subnetwork extracts the area around the heart (ROI) using morphological processing. Next, the second subnetwork segments the area into smaller and more defined parts. This enables reducing noise and achieving a Dice similarity coefficient (DSC) of 0.9119. To better align accuracy in segmentation with the ability of the method to be deployed in real-life clinical practice, Qu et al. (2022) developed a more lightweight cascading framework using a combination of slice filtering and attention methods. Unlike the in-plane anatomical restrictions noted by Zhang et al., the strategy proposed by Qu et al. uses slice selection on the Z-axis. The work relies on a lightweight standard convolutional neural network (T-CNN) acting as a classifier that can quickly detect the slices containing EAT and consequently reject many background slices at the input. In the next fine-segmentation stage, Qu et al. used RCA and ASPP in the U-Net framework, allowing the network to focus on fat tissue key features without the need for extra morphological post-processing. Qu et al. reported a DSC of 0.883 and an inference time of 2.65 seconds per case on their dataset. These results should not be interpreted as a head-to-head comparison with Zhang et al. All studies discussed underline that coarse-to-fine methodology, no matter whether by means of conventional anatomical ROI extractions or through implicit slice filtering, can support automated EAT estimation.

CMR fat segmentation can be challenging because of small targets, ambiguous local boundaries, and limited annotations. To tackle the problems of unclear borders and small datasets, Chen et al. (2023) [81] suggested a better version of the Triple-Stage Network (3SUnet). In contrast to Zhang et al., who extracted ROIs based only on the image features, Chen et al. implemented a multi-task continual learning strategy in the initial phase by employing segmentation and localization of the ventricles as auxiliary tasks. In particular, the model supports the identification of the ROI center using the prediction of the ventricle centroid and implements continual learning to apply anatomical prior knowledge from the external datasets (e.g., ACDC). In later stages, 3SU-net integrates ROI cropping and the Probability Map Generation Module to create a complete pipeline with multi-task localization, fine segmentation, and probabilistic refinement. Even in the challenging field of MRI, 3SUnet showed its best performance at 0.778 in DSC (F1 Score) and 3.476 in Hausdorff Distance and outperformed other techniques like U-Net with an F1 score of 0.732 and V-Net with an F1 score of 0.741. These results suggest that multi-task cascading architectures have distinct advantages in extracting very small and separate cardiac adipose depots.

4.5. Recurrent Neural Networks

Miller et al. used a ConvLSTM-based model to identify the cardiac silhouette on low-dose CT acquired with myocardial perfusion imaging; attenuation thresholds then defined EAT [59]. Model development used 500 patients, with 3511 patients held out for internal testing and 4770 for external testing. Against manual measurements, internal Spearman correlations were 0.90 for both EAT volume and attenuation; external correlations were 0.91 for volume and 0.82 for attenuation. Automated analysis took less than two seconds per scan, compared with approximately 15 min for manual annotation.

These approaches address different modeling requirements. U-Net variants provide segmentation backbones; attention and multi-scale modules refine feature extraction; CNN–Transformer and geometric methods explore broader spatial context; and state-space models offer another approach to long-range dependency modeling. Cascaded Dual U-Nets restrict segmentation to an anatomical region of interest, whereas ConvLSTM models encode relationships across adjacent slices. These categories should be distinguished, and their clinical suitability established through task-specific validation.

5. Discussion and Conclusions

As epicardial adipose tissue (EAT) has been recognized as a significant cardiovascular risk factor, automated quantification of this tissue has shifted from traditional segmented imaging techniques to using deep representation algorithms that include anatomical mechanisms as well as complex computational concepts to get high quality images. Convolutional neural networks, specifically U-Net and its three-dimensional iterations serve as the main

standard because they allow for effective volume measurements through CT and MRI methods. Using residual learning along with attention components helps these convolution models achieve better anatomical contours and fix the gap between low-level textures and high-level semantics. Moreover, to overcome segmentation perturbations such as the overlapping attenuation of EAT and paracardial fat, the employed multi-stage cascading methods and multi-task learning deliver crucial anatomical constraints. Coarse-to-fine cascading frameworks and collaborative learning networks which apply ventricle localization as an auxiliary goal reveal that the use of anatomical context for restricting the area of interest reduces chances of false positives and enhances robustness of the model across modalities even if there are no clear boundaries between tissues.

Hybrid CNN–Transformer models, Poincaré embeddings, and state-space architectures provide different ways to represent spatial context in cardiac images. Their reported applications remain tied to specific imaging protocols and anatomical targets. Further comparative evaluation is needed to determine whether these designs improve robustness or efficiency under the same training and testing conditions.

Generalization remains a central challenge for clinical deployment. Differences in scanner hardware, acquisition protocols, reconstruction, and patient populations can change the input distribution. External testing, transparent annotation definitions, and evaluation across institutions are therefore important. Domain adaptation and transfer learning are possible research directions, but should not be assumed to remove domain shift without validation in the intended setting.

Clinical integration also requires attention to memory use, inference time, and compatibility with existing workflows. Efficient model designs, pruning, quantization, and knowledge distillation are candidate engineering strategies; any reduction in computation should be evaluated alongside segmentation and measurement accuracy. MobileNet and EfficientNet provide general examples of efficient network design [82,83], but their use does not by itself establish clinical performance for EAT. Similarly, methods developed for other organs or classification tasks require EAT-specific validation before their benefits can be assumed. Progress toward routine EAT phenotyping depends on reproducible measurements, external validation, and evidence of incremental clinical value.

Despite various applicability limitations, several factors require consideration. One of the main limitations consists in the absence of standardized cross-modality annotations, since the boundary marking between epicardial adipose tissue and neighboring paracardial fat often depends on the operator's choice. In addition, deep learning algorithms tend to depend on some implicit presuppositions about the demographics and technologies used in the scanners being similar. Thus, the functioning of the algorithms may deteriorate in reference centers with different types of scanners, or in cases of studying a significant variety of adipose tissue population phenotypes. Identifying the nature of data and phenotypical factors is essential for the definition of practical limitations of automated systems used for quantification.

Author Contributions

J.T., Y.Z. and J.W.: literature search; J.T.: writing—original draft preparation, visualization; Q.Z.: visualization, supervision. All authors have read and agreed to the published version of the manuscript.

Funding

This research received no external funding.

Institutional Review Board Statement

Not applicable. This study exclusively used publicly available and anonymized datasets and did not involve direct recruitment of human participants or collection of identifiable patient information.

Informed Consent Statement

Not applicable.

Data Availability Statement

The datasets used in this study are publicly available. The corresponding data sources and access information are provided in the manuscript.

Conflicts of Interest

The authors declare no conflict of interest.

Use of AI and AI-Assisted Technologies

During the preparation of this work, the authors used ChatGPT (OpenAI) for language polishing and improving the readability of the manuscript. After using this tool/service, the authors reviewed and edited the content as needed and take full responsibility for the content of the published article.

References

1. GBD 2013 Mortality and Causes of Death Collaborators. Global, Regional, and National Age-Sex Specific All-Cause and Cause-Specific Mortality for 240 Causes of Death, 1990–2013: A Systematic Analysis for the Global Burden of Disease Study 2013. *Lancet* **2015**, *385*, 117–171. https://doi.org/10.1016/S0140-6736(14)61682-2.
2. Koenen, M.; Hill, M.A.; Cohen, P.; et al. Obesity, Adipose Tissue and Vascular Dysfunction. *Circ. Res.* **2021**, *128*, 951–968. https://doi.org/10.1161/circresaha.121.318093.
3. Song, Y.; Tan, Y.; Deng, M.; et al. Epicardial Adipose Tissue, Metabolic Disorders, and Cardiovascular Diseases: Recent Advances Classified by Research Methodologies. *MedComm* **2023**, *4*, e413. https://doi.org/10.1002/mco2.413.
4. Madonna, R.; Massaro, M.; Scoditti, E.; et al. The Epicardial Adipose Tissue and the Coronary Arteries: Dangerous Liaisons. *Cardiovasc. Res.* **2019**, *115*, 1013–1025. https://doi.org/10.1093/cvr/cvz062.
5. Konwerski, M.; Gąsecka, A.; Opolski, G.; et al. Role of Epicardial Adipose Tissue in Cardiovascular Diseases: A Review. *Biology* **2022**, *11*, 355. https://doi.org/10.3390/biology11030355.
6. Sacks, H.S.; Fain, J.N.; Bahouth, S.W.; et al. Adult Epicardial Fat Exhibits Beige Features. *J. Clin. Endocrinol. Metab.* **2013**, *98*, E1448–E1455. https://doi.org/10.1210/jc.2013-1265.
7. Sacks, H.S.; Fain, J.N.; Holman, B.; et al. Uncoupling Protein-1 and Related Messenger Ribonucleic Acids in Human Epicardial and Other Adipose Tissues: Epicardial Fat Functioning as Brown Fat. *J. Clin. Endocrinol. Metab.* **2009**, *94*, 3611–3615. https://doi.org/10.1210/jc.2009-0571.
8. Packer, M. Epicardial Adipose Tissue May Mediate Deleterious Effects of Obesity and Inflammation on the Myocardium. *J. Am. Coll. Cardiol.* **2018**, *71*, 2360–2372. https://doi.org/10.1016/j.jacc.2018.03.509.
9. Iacobellis, G.; Corradi, D.; Sharma, A.M. Epicardial Adipose Tissue: Anatomic, Biomolecular and Clinical Relationships with the Heart. *Nat. Clin. Pract. Cardiovasc. Med.* **2005**, *2*, 536–543. https://doi.org/10.1038/ncpcardio0319.
10. Pellegrinelli, V.; Carobbio, S.; Vidal-Puig, A. Adipose Tissue Plasticity: How Fat Depots Respond Differently to Pathophysiological Cues. *Diabetologia* **2016**, *59*, 1075–1088. https://doi.org/10.1007/s00125-016-3933-4.
11. Christensen, R.H.; von Scholten, B.J.; Hansen, C.S.; et al. Epicardial Adipose Tissue Predicts Incident Cardiovascular Disease and Mortality in Patients with Type 2 Diabetes. *Cardiovasc. Diabetol.* **2019**, *18*, 114. https://doi.org/10.1186/s12933-019-0917-y.
12. Pugliese, N.R.; Paneni, F.; Mazzola, M.; et al. Impact of Epicardial Adipose Tissue on Cardiovascular Haemodynamics, Metabolic Profile, and Prognosis in Heart Failure. *Eur. J. Heart Fail.* **2021**, *23*, 1858–1871. https://doi.org/10.1002/ejhf.2337.
13. Iacobellis, G. Epicardial Adipose Tissue in Contemporary Cardiology. *Nat. Rev. Cardiol.* **2022**, *19*, 593–606. https://doi.org/10.1038/s41569-022-00679-9.
14. Liu, Z.; Wang, S.; Wang, Y.; et al. Association of Epicardial Adipose Tissue Attenuation with Coronary Atherosclerosis in Patients with a High Risk of Coronary Artery Disease. *Atherosclerosis* **2019**, *284*, 230–236. https://doi.org/10.1016/j.atherosclerosis.2019.01.033.
15. Lenchik, L.; Heacock, L.; Weaver, A.A.; et al. Automated Segmentation of Tissues Using CT and MRI: A Systematic Review. *Acad. Radiol.* **2019**, *26*, 1695–1706. https://doi.org/10.1016/j.acra.2019.07.006.
16. Militello, C.; Rundo, L.; Toia, P.; et al. A Semi-Automatic Approach for Epicardial Adipose Tissue Segmentation and Quantification on Cardiac CT Scans. *Comput. Biol. Med.* **2019**, *114*, 103424. https://doi.org/10.1016/j.compbiomed.2019.103424.
17. Commandeur, F.; Goeller, M.; Betancur, J.; et al. Deep Learning for Quantification of Epicardial and Thoracic Adipose Tissue from Non-Contrast CT. *IEEE Trans. Med. Imaging* **2018**, *37*, 1835–1846. https://doi.org/10.1109/tmi.2018.2804799.
18. Gaborit, B.; Julla, J.B.; Fournel, J.; et al. Fully Automated Epicardial Adipose Tissue Volume Quantification with Deep Learning and Relationship with CAC Score and Micro/Macrovascular Complications in People Living with Type 2 Diabetes: The Multicenter EPIDIAB Study. *Cardiovasc. Diabetol.* **2024**, *23*, 328. https://doi.org/10.1186/s12933-024-02411-y.
19. Iacobellis, G.; Mahabadi, A.A. Is Epicardial Fat Attenuation a Novel Marker of Coronary Inflammation? *Atherosclerosis* **2019**, *284*, 212–213.
20. Nogajski, Ł.; Mazuruk, M.; Kacperska, M.; et al. Epicardial Fat Density Obtained with Computed Tomography Imaging-More Important than Volume? *Cardiovasc. Diabetol.* **2024**, *23*, 389. https://doi.org/10.1186/s12933-024-02474-x.
21. Iacobellis, G.; Secchi, F.; Capitanio, G.; et al. Epicardial Fat Inflammation in Severe COVID-19. *Obesity* **2020**, *28*, 2260–2262. https://doi.org/10.1002/oby.23019.
22. He, X.; Guo, B.J.; Lei, Y.; et al. Automatic Segmentation and Quantification of Epicardial Adipose Tissue from Coronary Computed Tomography Angiography. *Phys. Med. Biol.* **2020**, *65*, 095012. https://doi.org/10.1088/1361-6560/ab8077.
23. Hoori, A.; Hu, T.; Lee, J.; et al. Deep Learning Segmentation and Quantification Method for Assessing Epicardial Adipose Tissue in CT Calcium Score Scans. *Sci. Rep.* **2022**, *12*, 2276. https://doi.org/10.1038/s41598-022-06351-z.

24. Carr, J.J.; Ding, J. Response to "Epicardial and Pericardial Fat: Close, but Very Different". *Obesity* **2009**, *17*, 626–627. https://doi.org/10.1038/oby.2008.622.
25. Chhabra, L.; Kowlgi, N.G. Cardiac Adipose Tissue: Distinction between Epicardial and Pericardial Fat Remains Important! *Int. J. Cardiol.* **2015**, *201*, 274–275. https://doi.org/10.1016/j.ijcard.2015.08.068.
26. Rosito, G.A.; Massaro, J.M.; Hoffmann, U.; et al. Pericardial Fat, Visceral Abdominal Fat, Cardiovascular Disease Risk Factors, and Vascular Calcification in a Community-Based Sample: The Framingham Heart Study. *Circulation* **2008**, *117*, 605–613. https://doi.org/10.1161/circulationaha.107.743062.
27. Marwan, M.; Achenbach, S. Quantification of Epicardial Fat by Computed Tomography: Why, when and How. *J. Cardiovasc. Comput. Tomogr.* **2013**, *7*, 3–10. https://doi.org/10.1016/j.jcct.2013.01.002.
28. Sacks, H.S.; Fain, J.N. Human Epicardial Adipose Tissue: A Review. *Am. Heart J.* **2007**, *153*, 907–917. https://doi.org/10.1016/j.ahj.2007.03.019.
29. Iacobellis, G.; Assael, F.; Ribaudo, M.C.; et al. Epicardial Fat from Echocardiography: A New Method for Visceral Adipose Tissue Prediction. *Obes. Res.* **2003**, *11*, 304–310. https://doi.org/10.1038/oby.2003.45.
30. Antoniades, C.; Tousoulis, D.; Vavlukis, M.; et al. Perivascular Adipose Tissue as a Source of Therapeutic Targets and Clinical Biomarkers: A Clinical Consensus Statement from the European Society of Cardiology Working Group on Coronary Pathophysiology and Micro-Circulation. *Eur. Heart J.* **2023**, *44*, 3827–3844. https://doi.org/10.1093/eurheartj/ehad484.
31. Iacobellis, G. Epicardial and Pericardial Fat—Separated but under the Same Roof. *JAMA Cardiol.* **2024**, *9*, 949. https://doi.org/10.1001/jamacardio.2024.2424.
32. Iacobellis, G.; Bianco, A.C. Epicardial Adipose Tissue: Emerging Physiological, Pathophysiological and Clinical Features. *Trends Endocrinol. Metab.* **2011**, *22*, 450–457. https://doi.org/10.1016/j.tem.2011.07.003.
33. Marchington, J.M.; Mattacks, C.A.; Pond, C.M. Adipose Tissue in the Mammalian Heart and Pericardium: Structure, Foetal Development and Biochemical Properties. *Comp. Biochem. Physiol. Part B Comp. Biochem.* **1989**, *94*, 225–232. https://doi.org/10.1016/0305-0491(89)90337-4.
34. Greco, F.; Salgado, R.; Van Hecke, W.; et al. Epicardial and Pericardial Fat Analysis on CT Images and Artificial Intelligence: A Literature Review. *Quant. Imaging Med. Surg.* **2022**, *12*, 2075–2089. https://doi.org/10.21037/qims-21-945.
35. Rabkin, S.W. Epicardial Fat: Properties, Function and Relationship to Obesity. *Obes. Rev.* **2007**, *8*, 253–261. https://doi.org/10.1111/j.1467-789x.2006.00293.x.
36. Ansaldo, A.M.; Montecucco, F.; Sahebkar, A.; et al. Epicardial Adipose Tissue and Cardiovascular Diseases. *Int. J. Cardiol.* **2019**, *278*, 254–260. https://doi.org/10.1016/j.ijcard.2018.09.089.
37. Patel, V.B.; Shah, S.; Verma, S.; et al. Epicardial Adipose Tissue as a Metabolic Transducer: Role in Heart Failure and Coronary Artery Disease. *Heart Fail. Rev.* **2017**, *22*, 889–902. https://doi.org/10.1007/s10741-017-9644-1.
38. Hruskova, J.; Maugeri, A.; Podroužková, H.; et al. Association of Cardiovascular Health with Epicardial Adipose Tissue and Intima Media Thickness: The Kardiovize Study. *J. Clin. Med.* **2018**, *7*, 113. https://doi.org/10.3390/jcm7050113.
39. Mancio, J.; Azevedo, D.; Saraiva, F.; et al. Epicardial Adipose Tissue Volume Assessed by Computed Tomography and Coronary Artery Disease: A Systematic Review and Meta-Analysis. *Eur. Heart J. Cardiovasc. Imaging* **2018**, *19*, 490–497. https://doi.org/10.1093/ehjci/jex314.
40. Powell-Wiley, T.M.; Poirier, P.; Burke, L.E.; et al. Obesity and Cardiovascular Disease: A Scientific Statement from the American Heart Association. *Circulation* **2021**, *143*, e984–e1010. https://doi.org/10.1161/cir.0000000000000973.
41. Mahabadi, A.A.; Massaro, J.M.; Rosito, G.A.; et al. Association of Pericardial Fat, Intrathoracic Fat, and Visceral Abdominal Fat with Cardiovascular Disease Burden: The Framingham Heart Study. *Eur. Heart J.* **2009**, *30*, 850–856. https://doi.org/10.1093/eurheartj/ehn573.
42. Grodecki, K.; Lin, A.; Razipour, A.; et al. Epicardial Adipose Tissue Is Associated with Extent of Pneumonia and Adverse Outcomes in Patients with COVID-19. *Metabolism* **2021**, *115*, 154436. https://doi.org/10.1016/j.metabol.2020.154436.
43. Nagy, E.; Jermendy, A.L.; Merkely, B.; et al. Clinical Importance of Epicardial Adipose Tissue. *Arch. Med. Sci.* **2017**, *13*, 864–874. https://doi.org/10.5114/aoms.2016.63259.
44. Wong, C.X.; Ganesan, A.N.; Selvanayagam, J.B. Epicardial Fat and Atrial Fibrillation: Current Evidence, Potential Mechanisms, Clinical Implications, and Future Directions. *Eur. Heart J.* **2017**, *38*, 1294–1302. https://doi.org/10.1093/eurheartj/ehw045.
45. Geers, J.; Manral, N.; Park, C.; et al. AI-Quantified Epicardial Adipose Tissue and Prediction of Future Myocardial Infarction in Patients with Cardiometabolic Disease: A Post-Hoc Analysis from the SCOT-HEART Trial. *Cardiovasc. Diabetol.* **2025**, *24*, 403. https://doi.org/10.1186/s12933-025-02946-8.
46. Foldyna, B.; Hadzic, I.; Zeleznik, R.; et al. Deep Learning Analysis of Epicardial Adipose Tissue to Predict Cardiovascular Risk in Heavy Smokers. *Commun. Med.* **2024**, *4*, 44. https://doi.org/10.1038/s43856-024-00475-1.
47. Firouznia, M.; Molnar, D.; Edin, C.; et al. Head-to-Head Comparison between MRI and CT in the Evaluation of Volume and Quality of Epicardial Adipose Tissue. *Radiol. Cardiothorac. Imaging* **2025**, *7*, e240531. https://doi.org/10.1148/ryct.240531.
48. Feng, F.; Hasaballa, A.I.; Long, T.; et al. AI-Driven Segmentation and Morphogeometric Profiling of Epicardial Adipose Tissue in Type 2 Diabetes. *Cardiovasc. Diabetol.* **2025**, *24*, 294. https://doi.org/10.1186/s12933-025-02829-y.
49. Echols, J.T.; Wang, S.; Patel, A.R.; et al. Fatty Acid Composition MRI of Epicardial Adipose Tissue: Methods and Detection

of Proinflammatory Biomarkers in ST-Segment Elevation Myocardial Infarction Patients. *Magn. Reson. Med.* **2025**, *93*, 519–535. https://doi.org/10.1002/mrm.30285.

50. Duca, F.; Mascherbauer, K.; Donà, C.; et al. Association of Epicardial Adipose Tissue on Magnetic Resonance Imaging with Cardiovascular Outcomes: Quality over Quantity. *Eur. Heart J.* **2023**, *44*, ehad655.182. https://doi.org/10.1093/eurheartj/ehad655.182.
51. Skoda, I.; Henningsson, M.; Stenberg, S.; et al. Simultaneous Assessment of Left Atrial Fibrosis and Epicardial Adipose Tissue Using 3D Late Gadolinium Enhanced Dixon MRI. *J. Magn. Reson. Imaging* **2022**, *56*, 1393–1403. https://doi.org/10.1002/jmri.28100.
52. Zamani, S.K.; Aldiwani, H.; Razipour, A.; et al. Pericardial Fat from a Single Horizontal Long Axis Cardiac Magnetic Resonance Cine Image: A Validation Study against Three-Dimensional Cardiac Computed Tomography. *Eur. Heart J.* **2022**, *43*, ehac544.223. https://doi.org/10.1093/eurheartj/ehac544.223.
53. Iacobellis, G.; Willens, H.J. Echocardiographic Epicardial Fat: A Review of Research and Clinical Applications. *J. Am. Soc. Echocardiogr.* **2009**, *22*, 1311–1319. https://doi.org/10.1016/j.echo.2009.10.013.
54. Nerlekar, N.; Baey, Y.W.; Brown, A.J.; et al. Poor Correlation, Reproducibility, and Agreement between Volumetric versus Linear Epicardial Adipose Tissue Measurement. *JACC Cardiovasc. Imaging* **2018**, *11*, 1035–1036. https://doi.org/10.1016/j.jcmg.2017.10.019.
55. van Woerden, G.; van Veldhuisen, D.J.; Gorter, T.M. The Value of Echocardiographic Measurement of Epicardial Adipose Tissue in Heart Failure Patients. *ESC Heart Fail.* **2022**, *9*, 953–957.
56. Patra, P.; Bianchi, A.; Di Pompeo, D.; et al. Echocardiographic Epicardial Adipose Tissue Quantification: Challenges and Insights. In Proceedings of the 2024 IEEE International Conference on Pervasive Computing and Communications Workshops and Other Affiliated Events (PerCom Workshops), Biarritz, France, 11–15 March 2024; pp. 619–624. https://doi.org/10.1109/percomworkshops59983.2024.10502745.
57. Daudé, P.; Ancel, P.; Confort Gouny, S.; et al. Deep-Learning Segmentation of Epicardial Adipose Tissue Using Four-Chamber Cardiac Magnetic Resonance Imaging. *Diagnostics* **2022**, *12*, 126. https://doi.org/10.3390/diagnostics12010126.
58. Langenbach, I.L.; Hadzic, I.; Zeleznik, R.; et al. Association of Epicardial Adipose Tissue Changes on Serial Chest CT Scans with Mortality: Insights from the National Lung Screening Trial. *Radiology* **2025**, *314*, e240473. https://doi.org/10.1148/radiol.240473.
59. Miller, R.J.H.; Shanbhag, A.; Killekar, A.; et al. AI-Derived Epicardial Fat Measurements Improve Cardiovascular Risk Prediction from Myocardial Perfusion Imaging. *npj Digit. Med.* **2024**, *7*, 24. https://doi.org/10.1038/s41746-024-01020-z.
60. Guglielmo, M.; Penso, M.; Carerj, M.L.; et al. DEep LearnIng-Based QuaNtification of Epicardial Adipose Tissue Predicts MACE in Patients Undergoing Stress CMR. *Atherosclerosis* **2024**, *397*, 117549. https://doi.org/10.1016/j.atherosclerosis.2024.117549.
61. Bartoli, A.; Fournel, J.; Ait-Yahia, L.; et al. Automatic Deep-Learning Segmentation of Epicardial Adipose Tissue from Low-Dose Chest CT and Prognosis Impact on COVID-19. *Cells* **2022**, *11*, 1034. https://doi.org/10.3390/cells11061034.
62. Rodrigues, É.O.; Rodrigues, L.O.; Oliveira, L.S.N.; et al. Automated Recognition of the Pericardium Contour on Processed CT Images Using Genetic Algorithms. *Comput. Biol. Med.* **2017**, *87*, 38–45. https://doi.org/10.1016/j.compbiomed.2017.05.013.
63. Rodrigues, É.O.; Pinheiro, V.H.A.; Liatsis, P.; et al. Machine Learning in the Prediction of Cardiac Epicardial and Mediastinal Fat Volumes. *Comput. Biol. Med.* **2017**, *89*, 520–529. https://doi.org/10.1016/j.compbiomed.2017.02.010.
64. Tang, K.X.; Liao, X.B.; Yuan, L.Q.; et al. An Enhanced Deep Learning Method for the Quantification of Epicardial Adipose Tissue. *Sci. Rep.* **2024**, *14*, 24947. https://doi.org/10.1038/s41598-024-75659-9.
65. Theis, M.; Garajová, L.; Salam, B.; et al. Deep Learning for Opportunistic, End-to-End Automated Assessment of Epicardial Adipose Tissue in Pre-Interventional, ECG-Gated Spiral Computed Tomography. *Insights Imaging* **2024**, *15*, 301. https://doi.org/10.1186/s13244-024-01875-6.
66. Zhou, Z.; Rahman Siddiquee, M.M.; Tajbakhsh, N.; et al. UNet++: A Nested U-Net Architecture for Medical Image Segmentation. In *Deep Learning in Medical Image Analysis and Multimodal Learning for Clinical Decision Support*; Springer International Publishing: Cham, Switzerland, 2018; pp. 3–11. https://doi.org/10.1007/978-3-030-00889-5_1.
67. Leng, S.; Cheng, N.; Tan, E.; et al. Deep Learning-Based Quantification of Epicardial Adipose Tissue Volume from Non-Contrast Computed Tomography Images: A Multi-Centre Study. *Eur. Heart J. Digit. Health* **2025**, *6*, 1223–1233. https://doi.org/10.1093/ehjdh/ztaf116.
68. Qu, J.; Chang, Y.; Sun, L.; et al. Deep Learning-Based Approach for the Automatic Quantification of Epicardial Adipose Tissue from Non-Contrast CT. *Cogn. Comput.* **2022**, *14*, 1392–1404. https://doi.org/10.1007/s12559-022-10036-0.
69. Bard, A.; Raisi-Estabragh, Z.; Ardissino, M.; et al. Automated Quality-Controlled Cardiovascular Magnetic Resonance Pericardial Fat Quantification Using a Convolutional Neural Network in the UK Biobank. *Front. Cardiovasc. Med.* **2021**, *8*, 677574. https://doi.org/10.3389/fcvm.2021.677574.
70. Ye, H.; Deng, Y.; Hong, Y. Epicardial Adipose Tissue Segmentation in MRIs Using Text-Prompted Pretraining Model. In Proceedings of the 2024 IEEE International Conference on Bioinformatics and Biomedicine (BIBM), Lisbon, Portugal, 3–6 December 2024; pp. 7021–7028. https://doi.org/10.1109/bibm62325.2024.10822506.
71. Wang, Y.; Wang, A.; Wang, L.; et al. Automated Pericardium Segmentation and Epicardial Adipose Tissue Quantification from Computed Tomography Images. *Biomed. Signal Process. Control.* **2025**, *100*, 107167. https://doi.org/10.

1016/j.bspc.2024.107167.

72. Firouznia, M.; Ylipää, E.; Henningsson, M.; et al. Poincare Guided Geometric UNet for Left Atrial Epicardial Adipose Tissue Segmentation in Dixon MRI Images. *Sci. Rep.* **2025**, *15*, 25549. https://doi.org/10.1038/s41598-025-10110-1.
73. Kuo, L.; Wang, G.J.; Su, P.H.; et al. Deep Learning-Based Workflow for Automatic Extraction of Atria and Epicardial Adipose Tissue on Cardiac Computed Tomography in Atrial Fibrillation. *J. Chin. Med. Assoc.* **2024**, *87*, 471–479. https://doi.org/10.1097/jcma.0000000000001076.
74. Brendel, J.M.; Mayrhofer, T.; Hadzic, I.; et al. Sex-Specific Prognostic Value of Automated Epicardial Adipose Tissue Quantification on Serial Lung Cancer Screening Chest Computed Tomography. *Eur. Heart J. Cardiovasc. Imaging* **2025**, *26*, 1782–1792. https://doi.org/10.1093/ehjci/jeaf257.
75. Zhang, R.; Wang, X.; Zhou, Z.; et al. Epicardial and Paracardial Adipose Tissue Quantification in Short-Axis Cardiac Cine MRI Using Deep Learning. *Magn. Reson. Mater. Phys. Biol. Med.* **2025**, *39*, 97–108. https://doi.org/10.1007/s10334-025-01288-6.
76. Singh, P.; Hu, T.; Hoori, A.; et al. Sex-Specific Cardiovascular Risk Prediction Using AI-Derived Epicardial Adipose Tissue Measurements on CT Calcium Scoring Exams. *Am. J. Prev. Cardiol.* **2026**, *25*, 101367. https://doi.org/10.1016/j.ajpc.2025.101367.
77. Siriapisith, T.; Kusakunniran, W.; Haddawy, P. A 3D Deep Learning Approach to Epicardial Fat Segmentation in Non-Contrast and Post-Contrast Cardiac CT Images. *PeerJ Comput. Sci.* **2021**, *7*, e806. https://doi.org/10.7717/peerj-cs.806.
78. Zhang, Q.; Zhou, J.; Zhang, B.; et al. Automatic Epicardial Fat Segmentation and Quantification of CT Scans Using Dual U-Nets with a Morphological Processing Layer. *IEEE Access* **2020**, *8*, 128032–128041. https://doi.org/10.1109/access.2020.3008190.
79. Feng, F.; Carlhäll, C.J.; Tan, Y.; et al. FM-Net: A Fully Automatic Deep Learning Pipeline for Epicardial Adipose Tissue Segmentation. In *Statistical Atlases and Computational Models of the Heart. Regular and CMRxRecon Challenge Papers, Proceedings of the 14th International Workshop, STACOM 2023, Held in Conjunction with MICCAI 2023, Vancouver, BC, Canada, 12 October 2023*; Springer, Cham, Switzerland, 2024; pp. 88–97.
80. Xue, J.; He, K.; Nie, D.; et al. Cascaded Multitask 3-D Fully Convolutional Networks for Pancreas Segmentation. *IEEE Trans. Cybern.* **2021**, *51*, 2153–2165. https://doi.org/10.1109/tcyb.2019.2955178.
81. Chen, S.; An, D.; Feng, C.; et al. Segmentation of Pericardial Adipose Tissue in CMR Images: A Benchmark Dataset MRPEAT and a Triple-Stage Network 3SUnet. *IEEE Trans. Med. Imaging* **2023**, *42*, 2386–2399. https://doi.org/10.1109/tmi.2023.3251368.
82. Howard, A.G.; Zhu, M.; Chen, B.; et al. MobileNets: Efficient Convolutional Neural Networks for Mobile Vision Applications. *arXiv* **2017**, arXiv:1704.04861.
83. Tan, M.; Le, Q. EfficientNet: Rethinking Model Scaling for Convolutional Neural Networks. In Proceedings of the International Conference on Machine Learning, Long Beach, CA, USA, 9–15 June 2019; pp. 6105–6114.